J. Ullrich V.P. Shevelko (Eds.)

Many-Particle Quantum Dynamics in Atomic and Molecular Fragmentation

With 179 Figures

Springer

20 Fast p–He Transfer Ionization Processes: A Window to Reveal the Non-s^2 Contributions in the Momentum Wave Function of Ground–State He

H. Schmidt-Böking, V. Mergel, R. Dörner, H.J. Lüdde, L. Schmidt, T. Weber, E. Weigold, and A.S. Kheifets

20.1 Introduction

It is commonly believed that the He ground-state wave function is perfectly understood, since the theoretically determined He ground-state binding energy [1,2] is in excellent agreement with high-precision experimental data [3]. In investigating the ground-state binding energy by high-resolution spectroscopy one probes, however, the wave function at the region of the maximum density at a distance close to the Bohr radius. The theoretical binding energies are obtained on the basis of a many-body approximation, such as the multiconfiguration approach (MCA). Using variational methods, a wave function is generated that requires a huge basis of diagonal and off-diagonal matrix elements, or as in nuclear physics on-shell and off-shell states. These off-diagonal matrix elements represent highly correlated virtually excited contributions to the He ground state, which cannot be described by He independent-particle shell-model states, i.e., the lowest virtually excited p contributions for this He ground state are not the 2p states of He but are the so-called pseudostates [4–6] in the field of a nucleus with a nuclear charge larger than two. The MCA He ground-state wave function is then represented by a very long list of numbers, which account for the strength of all diagonal and off-diagonal matrix elements. Since the He ground state is a $^1S_0$ state, the three-particle ground state can contain only strongly correlated s^2, p^2, etc. $^1S_0$ contributions, and the MCA wave function can be separated into such angular-momentum contributions. In MCA ground-state energy calculations the s^2 states contribute about 99% of the energy, the virtually excited p^2 about 1%, etc.

Since the early days of atomic physics the correlated momentum wave function of the He ground state remained as one of the unsolved fundamental puzzles in modern physics [7]. Until recently, there was no experimental way to directly access the correlated momentum wave function of both electrons in the He ground state. Electron-momentum spectroscopy measurements to final He^+ ion states with symmetries, such as np, nd, etc., not contained in the Hartree–Fock ground state, provide such a method. However, in He^+ the $n\ell$ ($\ell \neq 0$, $n \geq 2$) states for a given n cannot be resolved, and since the ion ns states ($n \neq 0$) are not completely orthogonal to the He ground-state 1s

wave function excitation of these states is possible, even in the Hartree–Fock (s^2) approximation. Here n and ℓ denote the principal and orbital quantum numbers.

Cook et al. [8] used the technique of electron-momentum spectroscopy (e,2e measurements) to investigate the non-s components and found that the recoil-ion momentum distributions to the $n = 2$ states of He^+ were dominated by the correlated part of the He ground-state wave function. However, since they could not separate the 2p from the 2s states in their measurements, there was still a small s contribution to the cross section. Thus, although these highly correlated *virtually* excited states are usually believed to be merely mathematical constructs, which cannot be observed in experiments, suitable experiments can project them out. The direct observation of off-diagonal or non-s^2 contributions would reveal a scarcely explored, but very fundamental, part of the correlated momentum wave function of the He ground state. Other possible experiments that select the correlated part of the wave functions are photo double ionization (γ,2e) at high photon energies, when both electrons are emitted with similar high energy and can be treated as plane wave (see [9,10] and also [11] for a recent review).

Several groups have recently performed the so-called (e,3e) [12–17] experiments with He targets and have measured fully differential cross sections in momentum space. In (e,3e)-like experiments, where post-collision interaction is relatively small, indications of discrete structures in the final-state momentum pattern were found [12,14]. However, these experiments have been performed in the regime where one or more of the outgoing electrons has a very low energy, and therefore the reaction dynamics has been dominated by second-order and post-collision effects. In addition, they have no direct access to the initial-state momentum vector of one of the bound electrons. The relative importance of the non-s^2 contributions should increase towards larger distance from the nucleus and in the regime of high-momentum components of the wave function.

From the Schrödinger equation we learn that the ground-state wave function at large distance from the nucleus is the tunneling part. It is commonly believed that all bound electrons at large distance from the nucleus have to move slowly. This is true for Rydberg state electrons, but not for tunneling ground-state electrons. Here, electrons can still have high kinetic energy, since tunneling means no deceleration by the Coulomb potential $\propto 1/r$. The tunneling electron to absorb a virtual photon has for a very short time (see, e.g., self-energy process), to enable it to move fast to large distances. These non-s^2 contributions at large distance from the nucleus are important for the long-range properties of the He atom at low temperatures, in particular, to understand the weak van-der-Waals forces in the He ground state [15,16].

In the study presented here a particular channel of the transfer ionization (TI) process, the so-called correlated tunneling transfer ionization process (TuTI) in $p+He \rightarrow H^0+He^{2+}+e^-$ collisions is chosen. This capture process is

a Brinkman–Kramers-like process when electron and proton velocities match. The advantage of this experimental technique is that TuTI in the case of electron capture by a fast proton at very small deflection angles (regime of distant collisions), allows one a determination of the initial-state momentum vector of the captured electron and gives detailed information on the correlated momentum wave function of the three-particle He ground state. This projection technique is based on a sudden but gentle reaction with a small perturbation in momentum space, where both He electrons undergo correlated transitions from the almost unperturbed initial to the well-resolved final momentum states. In this reaction channel, the fast proton captures, by tunneling through the two-center Coulomb barrier, one electron of the He atom (named number 1) almost exclusively into its ground state, while the remaining He^+ ion is left in a virtually exited state from which it instantaneously fragments due to a shake-off process leaving electron 2 in a continuum state.

In fast collisions, the He atom is dissected essentially instantaneously (reaction time < 1 a.u. $\approx 2.4 \times 10^{-17}$ s and proton impact velocity $v_p \approx 2$–8 a.u., 1 a.u. $\approx 2.2 \times 10^6$ m/s). Since the force between the fast departing neutral H^0 and the remaining He^{1+} decreases rapidly, postcollision interaction between the projectile and the fragments is negligibly small. Thus, electron 2 is transferred from a virtually exited state to the real energy continuum in the final state with only a minor change of its initial momentum. Since the initial-state momentum of electron 1 can be determined from the final-state H^0 deflection angle (as shown below), the initial-state momentum correlation between electron 1 and 2 can be directly revealed from the final-state momentum distributions obtained for the TuTI reaction channel [18].

The cold target recoil ion momentum spectroscopy (COLTRIMS) technique, applied here, combines a very high momentum resolution with very high coincidence efficiency as is described in the reviews [19,20]. We will show that it provides the possibility of making quasi-snapshots of the correlated momentum wave function similar as using an ultrafast stroboscopic camera with a resolution of $< 10^{-17}$ s. With the COLTRIMS Reaction Microscope one can project the total wave function, but also tiny fractions (here less than one part in 10^8) of the total momentum wave function onto a special kinematical final state. Thus, one can probe details of the ground-state wave function not seen before.

The electron transfer to the projectile can proceed via different reaction channels:

- electron-electron-Thomas TI (eeTTI) [21–27],
- nucleus-electron-Thomas TI (neTTI) [28–30] and
- uncorrelated ionization of electron 2 and tunneling capture of electron 1 (n/eTuTI) (n/e indicates that the H^0 transverse momentum is due to the scattering at the nucleus resp. at the emitted electron).

While eeTTI always leads to a transfer ionization where the second electron is ejected, the capture of the n/eTuTI- and neTTI-process is accompanied by ionization of the second electron either by shake-off (SO) from mainly s^2 contributions or by an independent binary collision (S2) of the proton with the second electron. The shake-off process is highly dependent on the correlated part of the wave function, which is virtually excited to the continuum. The momentum distribution of the shake-off electron 2 and its shake-off probability depend strongly on the momentum state of electron 1. This effect on the shake-off probability is well established: if electron 1 is removed via Compton scattering, which averages over all momenta of electron 1, the shake-off probability is 0.8%. If, however, electron 1 is picked from the high momentum component of the initial state by high-energy photo absorption, the shake-off probability rises to 1.67% [31–37].

One would expect that if the initial momentum state of electron 1 is not defined (as, say, on the total cross sections) the momenta of shake-off electron 2, which is mainly the s-electron, should peak at zero momentum in the laboratory frame. If the momentum of electron 1 is large and well defined, the momentum of shake-off electron 2 may also be large and may even be well defined. Again, a related effect has been theoretically predicted for double ionization at very high photon energies, where a contribution from two fast electrons is expected [38]. If the fully differential cross sections for the TuTI process are measured, such transitions can indeed be interpreted as a shake-off process, where electrons 1 and 2 initially occupy a well defined entangled and virtually excited off-diagonal state. All TI processes such as eeTTI, neTTI, and n/eTuTI, followed by double scattering with the He nucleus, will lead to characteristic locations in the final-state momentum phase space. The maxima of the distributions of the longitudinal H^0 final-state momentum and, in particular, of the recoil momentum, provide a unique signature for the different TI channels, as will be detailed below.

In order to distinguish the different channels experimentally the projectile momentum transfer (the transverse and longitudinal component) has to be measured with an extremely high resolution of about 0.3 a.u. that corresponds to $\approx 10^{-5}$ of the projectile momentum, which can never be achieved with standard techniques, but can easily be achieved by the COLTRIMS technique, where in inverse kinematics the recoil momentum is detected. In Fig. 20.1 the expected TI peak locations of the recoil-momentum distribution projected onto the H^0 scattering plane are shown schematically for fast-proton impact. The separation of the recoil energy between the channels is only of the order of a few meV.

20.2 Experimental Technique

Using the high momentum resolution and high multi-coincidence efficiency of COLTRIMS, the complete final-state momentum distributions for fast, i.e.,

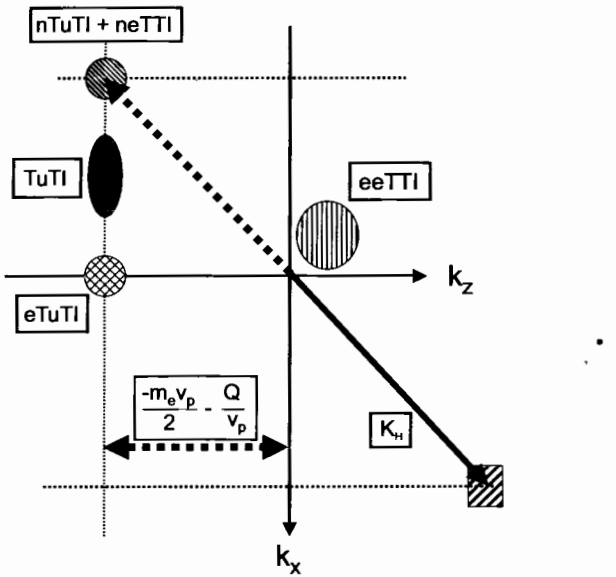

Fig. 20.1. Expected recoil-momentum locations for the different TI channels (neTTI, n/eTuTI, and eeTTI, for definitions see text) projected on the H^0 scattering plane. k_z defines the momentum components in the beam direction, k_x is the transverse momentum component in the direction of the scattered H^0. The *solid lines* represent $k_z = 0$, $k_x = 0$. k_H is the momentum change between initial and final state of the H particle. The *dashed lines* represent the positive and negative H transverse momenta and $-m_e v_p/2 - Q/v_p$ the He^{1+} recoil momentum in the lab frame for the pure electron capture into the H^0 ground state

with energy of 150 to 1400 keV collisions, transfer ionization processes (TI)

$$p + He \rightarrow H^0 + He^{2+} + e^-$$

have been systematically measured by Mergel [39] at the 2.5-MeV van-de-Graaf accelerator of the Institut für Kernphysik of the Universität Frankfurt.

The experimental setup is shown in Fig. 20.2 and is described in detail in [39]. The projectile beam was collimated to a diameter of < 0.5 mm and a divergence of < 0.25 mrad. The beam was charge-state selected in front and behind the target region by different sets of electrostatic deflector plates. A supersonic helium gas-jet is used as the target, as it combines the two most important features necessary for high-resolution recoil-ion spectroscopy: low internal temperature and localization of the target (diameter 5 mm). The helium gas is cooled to 14 K before it expands through a 30-μm nozzle into the source chamber. During the expansion the gas cools down to an internal temperature of < 50 mK. The gas-jet is formed by passing through a 0.7-mm skimmer, located 6 mm from the nozzle, resulting in a jet diameter of 5 mm at the intersection with the ion beam. A residual gas pressure without the

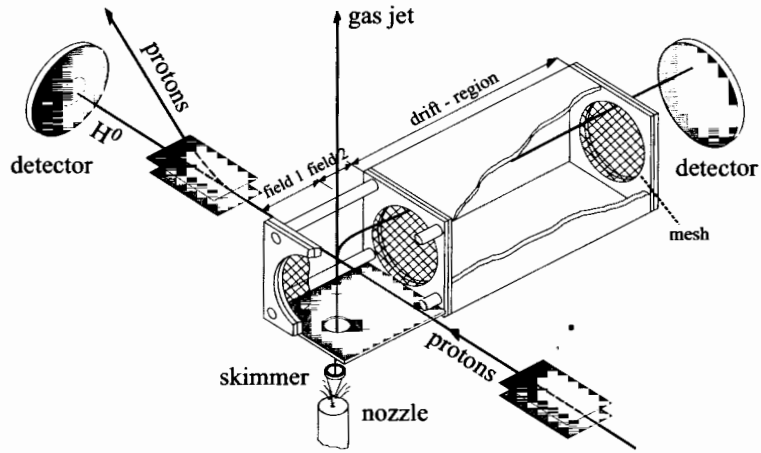

Fig. 20.2. Experimental setup of the COLTRIMS system with the H^0-recoil coincidence detection system

gas-jet of 1×10^{-8} mbar and a target density of 1.5×10^{12} were obtained. The recoil ions are extracted by a weak electric field of 9 V/cm transversely to the ion beam (see [19]). For this experiment we operated the spectrometer with a momentum resolution of 0.15 a.u. in favor of a higher target density.

The kinematics of the capture and TI reactions is described in detail in [19]. Here we repeat only the specific kinematical aspects of the two processes. In the TI process, the three free particles, diverging in the exit channel, have nine degrees of freedom. However, only five of them are independent, due to energy and momentum conservation. We have determined the polar and azimuthal scattering angle of the projectile in coincidence with the charge state and the 3-dimensional momentum vector of the recoiling target ion. Using the conservation laws, one obtains the 4-momentum components that have not been directly measured:[1]

$$k_{x,\mathrm{e2}} = -k_{x,\mathrm{H}} - k_{x,\mathrm{rec}}\,, \tag{20.1}$$

$$k_{y,\mathrm{e2}} = -k_{y,\mathrm{H}} - k_{y,\mathrm{rec}}\,, \tag{20.2}$$

$$k_{z,\mathrm{e2}} = v_\mathrm{P} \pm \sqrt{2(v_\mathrm{P}^2 + Q + v_\mathrm{P} k_{z,\mathrm{rec}}) - k_{x,\mathrm{e2}}^2 - k_{y,\mathrm{e2}}^2}\,, \tag{20.3}$$

$$k_{z,\mathrm{H}} = -k_{z,\mathrm{e2}} - k_{z,\mathrm{rec}}\,, \tag{20.4}$$

where $k_{x,\mathrm{rec}}$, $k_{y,\mathrm{rec}}$ and $k_{z,\mathrm{rec}}$ are the momentum components of the He^{2+}-recoil ion, $k_{x,\mathrm{e2}}$, $k_{y,\mathrm{e2}}$, and $k_{z,\mathrm{e2}}$ of the emitted electron and $k_{x,\mathrm{H}}$, $k_{y,\mathrm{H}}$ and $k_{z,\mathrm{H}}$

[1] A discussion of the kinematics of recoil ion production can also be found in [19]. The laboratory coordinate system and atomic units (e= $\hbar = m_e = 1$) are assumed here, where e and m_e denote the electron charge and mass, respectively, and $\hbar$ the Planck constant.

the momentum transfer of the projectile including the transferred electron with respect to the laboratory frame. x, y denote the components perpendicular and z the component parallel to the incident projectile, v_p the proton velocity. The Q-value is equal to $Q = E_\mathrm{He} - E_\mathrm{H}$, where E_H denotes the binding energy of the hydrogen atom and $E_\mathrm{He} = -2.9\,\mathrm{a.u.}$ that of the helium ground state. Exploiting the rotational symmetry we rotate the coordinate frame around the z-axis from the laboratory frame into the scattering plane, defined by the incident and scattered projectile for each event. x and y denote the components parallel and perpendicular to the projectile scattering plane, where the projectile is scattered in the positive x-direction. This is equivalent to the definition of $\mathrm{k}_{y,\mathrm{H}} = 0$ for each event.

Equation (20.3) contains two unknown quantities:

- the final binding energy of the hydrogen bound state E_H that is included in the Q-value, and
- the sign of the square root.

Because the capture leads predominantly to the ground state of hydrogen [42] we use the value of $Q = -2.4\,\mathrm{a.u.}$ In addition to that, the error in $k_{z,\mathrm{e2}}(\Delta k_{z,\mathrm{e2}})$ is of the order of $\Delta Q/v_\mathrm{P}$, where the maximum error in Q is $\Delta Q = 0.5\,\mathrm{a.u.}$ Thus, for the investigated projectile velocities this gives $0.07 < \Delta k_{z,\mathrm{e2}} < 0.20$, which is in the range of the experimental resolution.

Concerning the sign in (20.3), we use the negative one for the calculation of $k_{z,\mathrm{e2}}$, since only electrons with $k_{z,\mathrm{e2}} > v_\mathrm{P}$ correspond to the positive sign. The contribution of electrons with $k_{z,\mathrm{e2}} > v_\mathrm{P}$ is in the range of 1% to 3% of the total cross section [43], thus this approximation does not significantly affect the calculated electron distributions. The resolution of $k_{z,\mathrm{e2}}$ due to calculation by (20.3) is $\Delta k_{z,\mathrm{e2}} = \pm 0.2\,\mathrm{a.u.}$ in the best case ($E_p = 0.15\,\mathrm{MeV}$), and $\Delta k_{z,\mathrm{e2}} = \pm 0.3\,\mathrm{a.u.}$ for the worst case ($E_p = 1.4\,\mathrm{MeV}$).

20.3 Experimental Results and Discussion of Observed Momentum Patterns

Our study of the TI process in p-He collisions was stimulated by the systematic work of Horsdal et al. [44] and Giese et al. [45] on TI processes for proton impact on He, who found a pronounced peak at about 6.5×10^{-4} rad in the H^0 scattering dependent ratio of TI to pure capture differential cross section. The peak maximum increased with projectile energy and reached about 25% at 1 MeV proton impact energy. Their observation contradicted all expectations, and was indeed very puzzling. Horsdal et al. explained their findings by a possible large contribution of eeTTI processes, whereas Olson et al. [46] as well as Gayet and Salin in their papers [43,47,48] showed (using CTMC and quantum-mechanical calculations in the independent-electron approximation) that multiple scattering might also produce such peak structures. Based on complete differential final-state momentum distributions, Mergel

et al. [18] could clearly show that neither eeTTI nor multiple scattering is responsible for the observed peak in the cross section ratio, but could not present an explanation for this peak structure. As Mergel et al. [18] have shown, the main contributions to TI for the projectile velocities investigated here and thus also the puzzling structures observed by Horsdal et al. result from the highly correlated TuTI process.

The complete differential cross sections in momentum space of [18,39] show some even more puzzling features of the momentum patterns, namely:

1. Electron 2 is predominantly emitted into the backward and negative k_x direction, i.e. the emission of electron 2 with respect to the outgoing H^0 is completely asymmetric.
2. The He^{2+} ion momentum distribution and, therefore, also the electron 2 distribution peak in the H^0 scattering plane.
3. The ratio of TuTI to pure capture total cross sections increases with decreasing perturbation, i.e. increasing proton impact energy.
4. Electron 1, recoil He^{2+}, and electron 2 always share comparable momenta. In particular, none of these particles in the final state shows a momentum distribution peaking at zero momentum at the laboratory frame. According to theoretical predictions [40] and [41], the momentum of shake electron 2 should peak at zero and the recoil k_r momentum would be expected to peak near $k_r = (0, 0, -v/2)$.

As was shown in [18], these four features cannot be explained by noncorrelated particle dynamics of a proton interacting with a He nucleus and two uncorrelated s electrons. In particular, observation 2., i.e., the four-particle planar final-state motion, requires a strong four-particle correlation in angular momentum. This angular momentum must already be present in the initial He ground state, since the momentum transfer of the proton to the He is small and, thus, also the angular momentum transfer is small, i.e., $\ll 1$ a.u. This conclusion is supported by the observation that at high E_p electron 1 is nearly exclusively captured into the projectile 1s state and in the pure capture channel electron 2 is very rarely excited into any higher $He^+(n\ell)$ state. We will show below that the TuTI process for the proton-impact energies investigated here proceeds nearly exclusively via shake-off processes from correlated non-s^2 contributions to the He ground state. Thus, the fragmentation of the He^{1+} ion always occurs due to the angular momentum entanglement of the three He particles and not by an uncorrelated interaction of the proton with electron 2. From the final-state momentum pattern of H^0, He^{2+} and the electron 2 we can deduce and directly reveal the part of the initial momentum wave function that is dominated by non-s^2 contributions.

To compare our data with previous measurements we have to integrate our data over some degrees of freedom, since no fully differential cross sections for TI processes in momentum space have been reported previously. In Fig. 20.3, the total TI cross sections are plotted as a function of the proton-impact

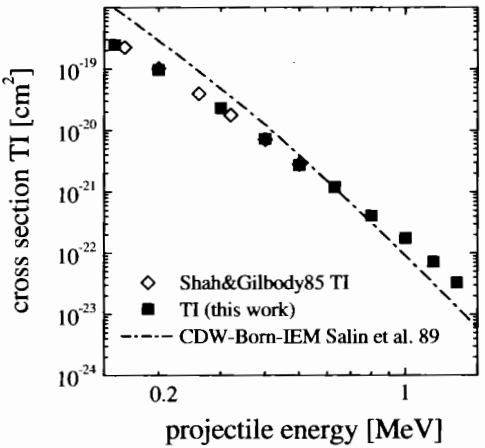

Fig. 20.3. Total TI cross sections as function of proton-impact energy

energy and compared with other published data [49]. The present data are in very good agreement with the earlier results.

In Fig. 20.4, we show the single differential TI (right column) together with the corresponding pure capture (left column) cross sections as a function of the H^0 transverse momentum k_{x,H^0} (i.e., the scattering angle θ_P) for different proton impact energies from 150 to 1400 keV. Within the experimental uncertainty, these data agree with the results presented by Horsdal et al. [50].

Plotting the ratio between TI and single capture cross sections as a function of the H^0 scattering angle (i.e., $k_{x,H^0}/k_0$) we find (see Fig. 20.5, open squares) the same narrow peak structure at about 0.65 mrad as reported by Giese and Horsdal [45] (solid circles). One observes in both experiments that the peak ratio slightly increases with projectile energy.

In Fig. 20.6 the ratios of total cross sections between TI and the sum of TI plus pure capture are plotted. Below $E_p = 600$ keV the ratio remains constant at about 2.5% in good agreement with the earlier data of Shah et al. [49]. Above $E_p = 600$ keV, however, the ratio increases linearly to about 4% for $E_p = 1.4$ MeV in agreement with recent data of [51]. Above 1400 keV it starts to decrease again towards higher energies [51]. Such a proton energy dependence for the total cross section ratio (smooth peak at about 1 MeV) is indeed unexpected. If electron 2 has to be emitted by any uncorrelated two-step process with the proton, we would expect a ratio similar to the result for pure He double to single ionization (open triangles) [45,52]. In both papers a ratio for the pure ionization channels far below 1% was found at 1 MeV, which decreases with increasing proton energy, since the perturbation by the proton decreases with increasing E_p. This comparison shows that the present measured ratio is in clear contradiction to that reported for the uncorrelated

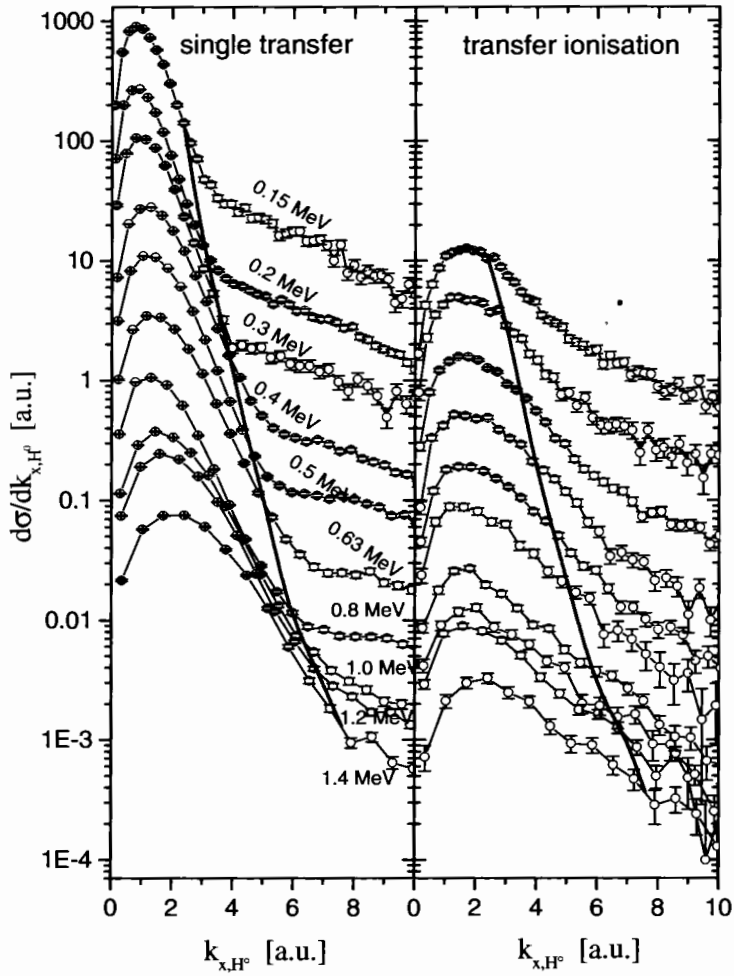

Fig. 20.4. Single differential TI cross sections $d\sigma/dk_{x,H^0}$ (*right column*) together with the corresponding pure capture cross sections (*left column*) as a function of the H^0 transverse momentum $k_{x,H}$ for different projectile energies

double-ionization processes. This supports our argument that the mechanism behind TuTI is mediated by strong electron correlation and not by two-step processes.

Considering the H^0 scattering-angle-dependent differential cross section for capture and TI (see Fig. 20.4), we see that both results show a large peak at very small scattering angles (below 0.6 mrad) and a smooth decrease of the cross sections above 1 mrad. This small-angle peak accounts for nearly all protons scattered by electrons of the He atom. This explanation has been

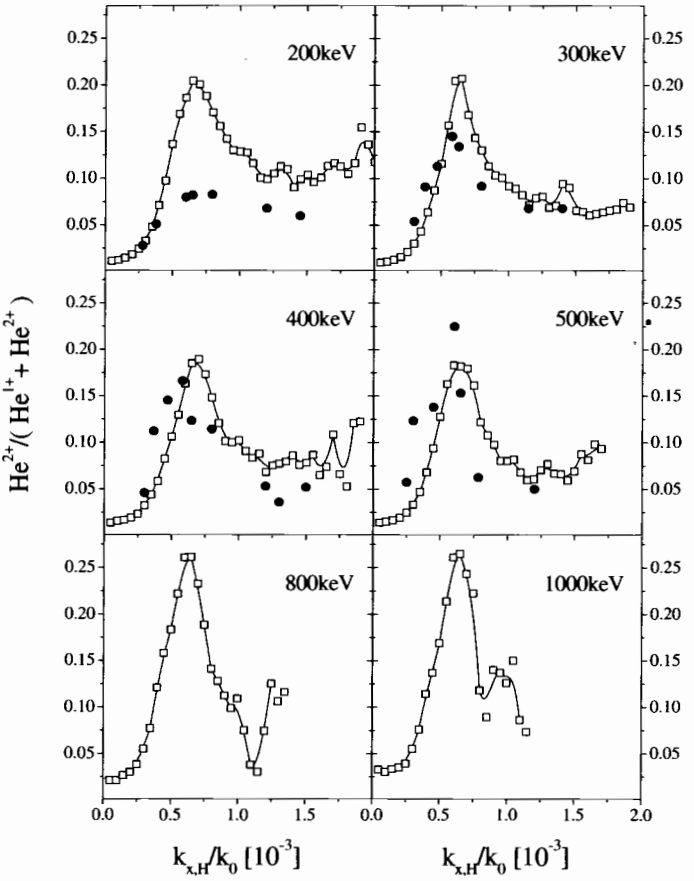

Fig. 20.5. H^0 scattering angle θ_P tatios of TI differential cross sections (this work, *open squares* and Giese and Horsdal, *solid circles*) to the sum of pure capture plus TI cross sections for different projectile energies. $\theta_P = k_{x,H}/k_0$, where $k_{x,H}$ is the H^0 transverse momentum and k_0 is the incoming projectile momentum

proven by calculations in which the nuclear-nuclear repulsion has been neglected [43,47,48]. As a result, the small scattering angle part of the capture cross section remains almost unchanged in the relative H^0 scattering angle dependence and the shape of each peak reflects the electron transverse velocity distribution for the given proton velocity v_p.

To present more evidence for the creation of the small-angle peak by proton scattering on the electrons, the data of DeHaven et al. [54] are presented in Fig. 20.7. The authors of [54] have investigated uncorrelated double-collision processes for the pure ionization channel of fast protons on He. In Fig. 20.7 the measured relation between the recoil transverse momentum $k_{x,\mathrm{rec}}$ and the

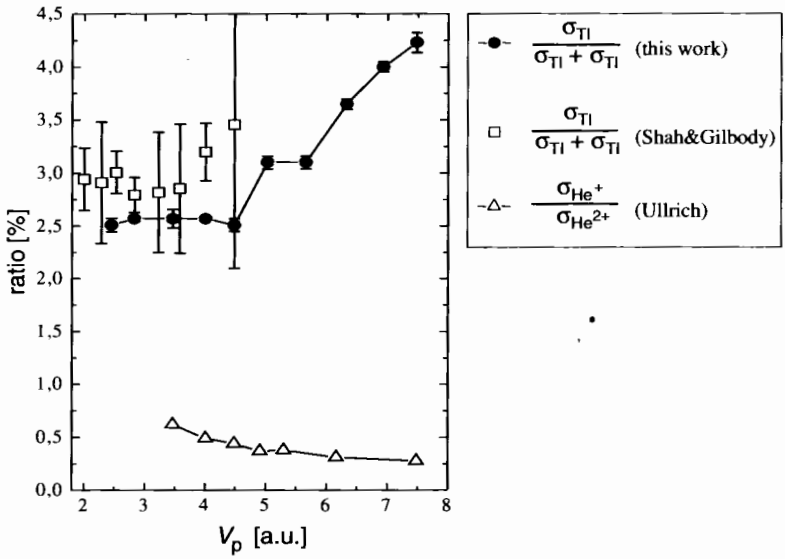

Fig. 20.6. Ratios of total TI cross section σ_{TI} to the sum of σ_{TI} and total single capture cross section σ_{SC}, *solid circles* and *open squares* (this work and [49]), ratio of total cross section of He^{2+} to He^{+} production, *open triangles* (Kristensen et al. [53] and Ullrich et al. [52]), as a function of proton impact velocity v_p

projectile scattering angle θ_{p} is shown. For small angles they observe that the projectile transverse momentum $k_{x,\mathrm{p}} = \theta_{\mathrm{p}} m_{\mathrm{p}} v_{\mathrm{p}}$ results exclusively from close collisions with the electrons (vertical line at $k_{x,\mathrm{rec}} = 0$). Due to the small ratio of electron-to-proton mass, the maximum angle of proton scattering by a free electron is 0.55 mrad. The nuclear momentum exchange (diagonal solid line) is for small θ_p much less probable but extends out to 180°. In the very small angle regime (the region of the peak) for most collisions the transverse nuclear-momentum exchange is below 0.2 a.u.. For Coulomb scattering at impact energies below 1 MeV this corresponds to impact parameters larger than the He K-shell radius. From the nuclear-transverse momentum exchange (relation between recoil and projectile) we thus obtain information on the nuclear-impact parameter range and indirectly also on the distance (close or distant) from the He nucleus where electron 1 is captured.

In the capture channel below 6×10^{-4} rad the H^0 transverse momentum is thus nearly exclusively determined by momentum transferred by the captured electron. For uncorrelated processes the probability that the proton shares comparable momentum with both the electron and the recoil ion is small (Fig. 20.7: the region between the two dashed-dotted lines). This behavior is well predicted by the small-angle multiple-scattering theory [55]. For the scattering of a proton from single atoms or thin solid targets even small

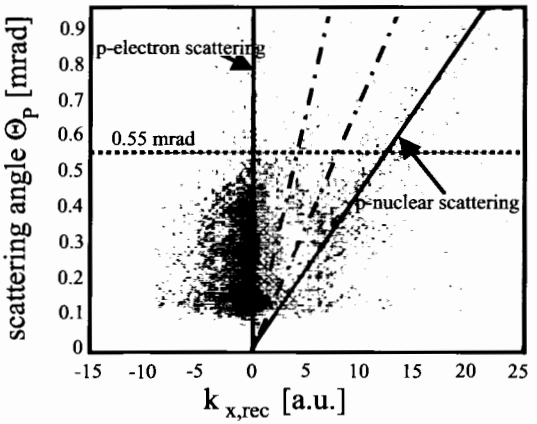

Fig. 20.7. Single ionization of He by 6 MeV proton impact He(p,p+e)He^+ measured by DeHaven et al. (adapted from [54]). Density plot of one component of the recoil transverse momentum $k_{x,\mathrm{rec}}$ vs. the projectile scattering angle θ_p. The *vertical solid line* represents H^0 scattering on the He electrons, where the recoil ion is a spectator and the diagonal solid line represents nuclear–nuclear transverse momentum exchange, when the electrons are spectators. The area between the *dashed-dotted lines* indicates the area where for the TuTI channel the measured recoil momenta are located

angle proton deflection is exclusively due to one close encounter with either an electron or a nucleus. The probability for the proton to be deflected by an angle θ_p on a single He atom by multiple scattering compared to single close-encounter scattering is always very small, since uncorrelated multiple scattering can go in any direction. Thus we can conclude that in uncorrelated processes equal momentum sharing of the proton with the emitted electron and the recoil is negligibly small.

For the discussion of the fully differential final-state momentum pattern of the TuTI, a coordinate system is defined where the z-axis is directed along the incoming projectile momentum $k_0 = m_\mathrm{p} v_\mathrm{p}$ and the H^0 projectile is always scattered into the positive x-direction. This coordinate system is obtained by rotating the laboratory frame around the z-axis so that the y-component of the projectile momentum $k_{y,\mathrm{H}}$ is always set to zero for each measured coincidence event. The solid lines in Figs. 20.8, 20.9 and 20.10 define the k_x and k_z zero positions.

The proton at large nuclear impact parameters would remain nearly non-deflected by the He nucleus, but the tunneling electron 1 carries some transverse momentum that has to be compensated by the outgoing H^0. When electron 1 approaches the proton with momentum $k_{x,\mathrm{e1}}$, the deflected H^0 must conserve this component, thus being deflected by $k_{x,\mathrm{H}} = k_{x,\mathrm{e1}}$. Since for kinematical capture the longitudinal momentum component of the initial-state electron velocity should match the projectile velocity (overlap with the

Compton profile of the 1s state of H^0), the initial-state momentum vector k_{el} of electron 1 can be approximately determined from the measured data by

$$\boldsymbol{k}_{el} = \begin{pmatrix} k_{el,x} \\ k_{el,y} \\ k_{el,z} \end{pmatrix} = \begin{pmatrix} k_{x,H} \\ 0 \\ v_p \end{pmatrix} . \tag{20.5}$$

For the pure capture channel the maximum transverse momentum of H^0 due to scattering on the electron is therefore $k_{x,H} \approx m_e v_p$, in nearly perfect agreement with the data. For the TuTI process the proton is scattered from a correlated electron pair (a quasi-heavy boson) thus the peak regime of θ_P can extend to about 1 mrad, which is twice the angle of the maximum deflection by a single electron.

The recoil momentum in the beam direction $k_{z,rec}$ can be expected to be close to that for pure single capture. This momentum, which is given by energy and momentum conservation is

$$k_{z,He^+} = -m_e v_p/2 - Q/v_p , \tag{20.6}$$

where $Q = -2.9$ a.u. (see [19,39] for the kinematics). This k_{z,He^+} value is indicated by the dashed lines in Figs. 20.8 and 20.9. This equation can be interpreted in the following way: The He^+ recoil in the initial state has a $k_{z,rec}$ momentum of $-m_e v_p$ in order to balance the momentum of the forward directed electron 1. In respect to the laboratory frame, the electron 1 after being captured gains the kinetic energy $m_e v_p^2/2$. Furthermore, due to that process the electronic binding energy is changed by $-Q = E_H + E_{He^+} - E_{He}$. The energy $m_e v_p^2/2 + Q$ must be provided by the kinetic energy of the proton and therefore leads to an energy loss or gain of the projectile. In a tunneling process (virtual photon exchange) projectile and recoil must undergo in their center-of-mass a symmetric energy-gain or loss process to conserve energy and momentum. This yields for the z-component of the recoiling ion $k_{z,He^+} = -(m_e v_p^2/2 - Q)/v_p$ as given in formula 20.6 and for the projectile $k_{z,H^0} = +(m_e v_p^2/2 - Q)/v_p$. Thus, the total relative longitudinal momentum change between recoil and H^0 in the final state is $m_e v_p$. In a TTI process, however, the momentum exchange is a sequence of close binary Coulomb collisions and the recoil yields a completely different momentum pattern in the final state compared to TuTI processes.

After the capture of the first electron in the TuTI process the He^+ fragments into the nucleus and a free electron 2. The momentum projections presented in Figs. 20.8, 20.9, and 20.10 are obtained by a smoothing procedure of the measured statistical distributions. The shading represents the numbers of measured counts in a linear scale normalized to the maximum intensity. The absolute scale varies from figure to figure and can be obtained for each data set from Fig. 20.4, where absolute cross sections for each angle and impact energy E_p are given. Thus for small angles and for small E_p the count rate is highest.

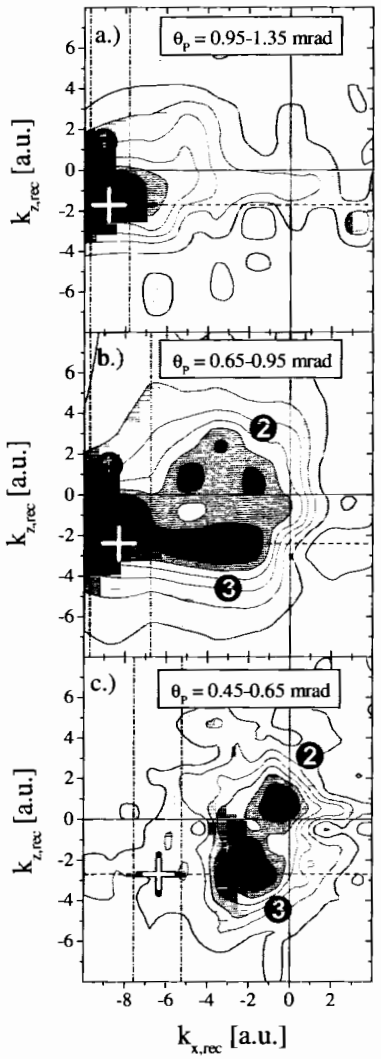

Fig. 20.8. Fully differential recoil ion TI cross sections projected on the H^0 scattering plane for selected projectile velocities and H^0 transverse momenta (**a**: 0.5 MeV, **b**: 0.8 MeV, **c**: 1 MeV). The *solid lines* represent $k_z = 0$, $k_x = 0$, the *dashed lines* the He^{1+} recoil momentum in the laboratory frame for the pure electron capture into the H^0 ground state, the areas between the *dashed-dotted lines* the window for the negative H^0 transverse momenta, the "+" cross the location calculated by the CTMC method for the channels neTTI and nTuTI. The locations of the observed peaks 1, 2, and 3 are discussed in the text

To prove the correctness of our momentum measurements, we first present data on those TI channels whose kinematics is well understood. In Fig. 20.8 data for large H^0 angles are shown, where transverse nuclear momentum exchange dominates. Only one recoil peak is seen and all recoil momenta are close to the location (+) predicted by CTMC calculations [21] for uncorrelated neTTI and n/eTuTI processes. The recoil momentum location agrees well with the expected location, but it is slightly shifted by about 1a.u. in the forward direction k_z (longitudinal position). This small forward shift is expected, since the nuclear scattering is probably accompanied by an in-

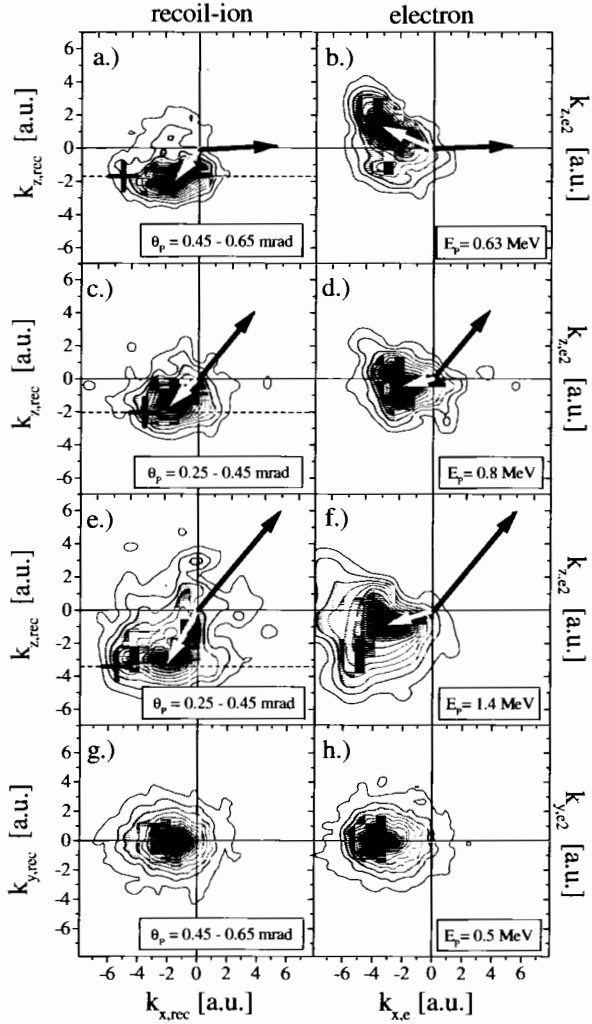

Fig. 20.9. Fully differential recoil ion (*left column*) and electron (*right column*) TI cross sections projected on the H^0 scattering plane for 630 keV impact energy at $\theta_P = 0.45$–0.65 mrad (**a,b**), in (**c,d**) for 800 keV $\theta_P = 0.25$–0.45 mrad, and in (**e,f**) for 1400 keV $\theta_P = 0.25$–0.45 mrad. The *solid lines* represent $k_z = k_x = 0$, the *dashed lines* the He^{1+} recoil momentum in the laboratory frame for the pure electron capture into the H^0 ground state. The *black vectors* indicate the mean electron 1 momentum vector in the initial state (20.7), the *white vectors* represent the mean measured recoil momenta, the "+" cross the expected location of neTTI and nTuTI channels. In (**g,h**) the differential recoil and electron cross sections perpendicular to the beam direction are shown

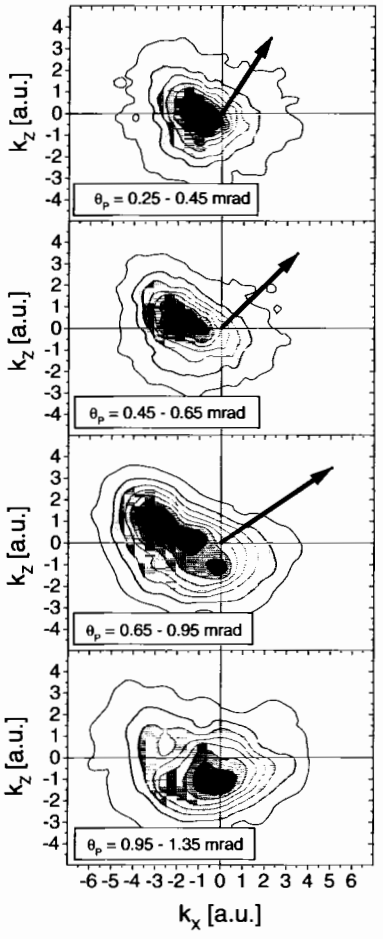

Fig. 20.10. Fully differential electron TI cross sections projected on the H^0 scattering plane for 300 keV impact energy at different H^0 scattering angles (for explanation see Fig. 20.9)

dependent very small angle TuTI process, where the electron 2 is emitted slightly backward. The areas between the dashed-dotted lines represent the window corresponding to the negative H^0 transverse momenta. In Fig. 20.8 data for those H^0 angle are shown, where several TI channels can contribute. Indeed three peaks are seen, peak 1 represents the nTuTI and neTTI channel near the expected location (+), where again the H^0 transverse momentum results from nuclear scattering. Peak 2 represents the electron–electron Thomas channel (eeTTI), (see Mergel et al. [21]). Its measured kinematical location also agrees well with the expected values. For eeTTI the recoil ion is mainly a spectator and the recoil momentum location is expected at small positive k_z and small negative k_x, in agreement with our measurement. In Fig. 20.8c, the data for the small H^0 angular regime are shown, where the proton is mainly scattered by electron 1. Two peaks are seen, one at $k_x = -1$ a.u.,

$k_z = +1$ a.u., which is the eeTTI channel [21]). The peak 3 in Fig. 20.8c, like the peak 3 in Fig. 20.8b, represents the TuTI channel. Their locations are contrary to the predictions for any known uncorrelated TI process, which should be located between the dashed-dotted lines.

Further results are shown in Fig. 20.9 where the corresponding fully differential recoil ion (left column) and electron (right column) cross sections projected on the H^0 scattering plane are presented. (In Fig. 20.9a and b for 630 keV impact energy at $\theta_p = 0.45$–0.65 mrad, in Fig. 20.9c and d for 800 keV at $\theta_p = 0.25$–$0{,}45$ mrad, and in Fig. 20.9e and f recoil and electron 2 momenta for 1400 keV at $\theta_p = 0.25$–$0{,}45$ mrad). Since for both the recoil ion and the electron one observes momentum distributions that are not rotationally symmetric with respect to k_{e1}, momentum exchange of the proton with the α nucleus and electron 2 must be correlated. It is obvious from Fig. 20.9 that the recoil and electron mean momenta have well-localized positions in the H^0 scattering plane. Furthermore both azimuthal momentum distributions peak always in the H^0 scattering plane. This is evident from Fig. 20.9g and h, where the corresponding azimuthal angular distributions of recoil and electron 2 momenta for a typical case of $E_p = 500$ keV are plotted.

In Fig. 20.10, the final-state momentum distributions of electron 2 are shown for 300 keV proton energy at different H^0 scattering angles. The black vectors in Figs. 20.9 and 20.10 indicate the momentum vector of electron 1 in its initial state calculated from (20.7), the white vectors indicate the corresponding recoil vectors (laboratory frame), respectively. From the discussions above we can conclude:

- The data presented here are reliable within the quoted error bars of about < 0.5 a.u.
- Besides the well-known TI channels we observe a TI channel, called TuTI, whose kinematics cannot be explained by any previously known TI mechanism.

20.4 Shake-Off Process From Non-s^2 Contributions

Before we discuss the measured fully differential momentum distributions, the shake-off ratios, i.e., ratios between TI and single-capture differential cross sections as function of the H^0 scattering angle, given in Fig. 20.5, will be compared with the theory presented in [40].

As in the standard shake-off theory [41], we estimate the probability of the cKTI process as a double overlap integral:

$$\langle \boldsymbol{k}_1 \boldsymbol{k}_2 | \Phi_0 \rangle = \sum_{nl} C^{00}_{lm,l-m} \langle \boldsymbol{k}_1 | nlm \rangle \langle \boldsymbol{k}_2 | nl - m \rangle \,, \tag{20.7}$$

where m denotes the projection of the orbital momentum ℓ. Here we make a multi-configuration Hartree–Fock expansion of the wave function of the

He atom ground state. Configuration interaction coefficients decrease rapidly with increasing n, l, the leading terms being $A_{1s} = 0.996$, $A_{2s} = -0.059$, $A_{2p} = 0.059$, $A_{3d} = -0.012$. The Clebsch–Gordan coefficients couple the two individual electron angular momenta to the zero angular momentum of the He atom. In the first overlap integral, we assume that the electron is picked up by the proton at a finite distance from the He nucleus:

$$\langle \boldsymbol{k}_1 | nlm \rangle = C_{lm} \int_{b>0}^{\infty} \mathrm{d}x \, \mathrm{e}^{k_{1x}x} \int_{-\infty}^{\infty} \mathrm{d}z \, \mathrm{e}^{k_{1z}z} \, R_{nl}(r) \, \mathrm{e}^{\mathrm{i}m\phi} \,, \tag{20.8}$$

where b is the impact parameter. Here we also choose the angular momentum quantization axis in the y-direction and write the electron wave function in the scattering plane as

$$\Psi_{nlm}(r) = R_{nl}(r) \, Y_{lm}(\theta = \pi/2, \phi) = C_{lm} R_{nl}(r) \, \mathrm{e}^{\mathrm{i}m\phi} \,, \quad \tan\phi = x/z \,.$$

In the second overlap $\langle \boldsymbol{k}_2 | nl - m \rangle$, the integration is expanded over the whole scattering plane and the final state $\langle \boldsymbol{k}_2 |$ is treated as the Coulomb wave in the He^{2+} field.

In the standard shake-off theory, the x integration in (20.8) is expanded over the whole scattering plane and the integral becomes symmetric with respect to the sign reversal of m. In the TuTI theory there is a very large asymmetry between $\pm m$ components $\langle \boldsymbol{k}_1 | nlm \rangle / \langle \boldsymbol{k}_1 | nl - m \rangle \propto k_{1z} b \propto 1$. This asymmetry can be understood if one remembers that the departing electron carries away the classical angular momentum $k_{1z} b$ and the projection of this momentum on the quantization axis favors only one particular sign of m. The large angular momentum $k_{1z} b \gg 1$ has to be drawn from a ground-state orbital with a limited l, m. This makes the overlap integral exponentially small $\langle \boldsymbol{k}_1 | nlm \rangle \propto \exp(-k_{1z} b)$. This smallness is offset by a growing power term $(\beta b)^1$ where β is the exponential fall-off parameter of the radial orbital $R_{nl}(r)$ (see [40] for more details). The power term compensates the small coefficients A_{nl} for $l > 0$. As a result, the strongest contribution to the amplitude equation (20.8) comes from the $2p_{+1}$ and $3d_{+2}$ terms but not the 1s one.

In Fig. 20.11 (right column) the experimental ratios for 500 and 1000 keV proton impact energy are shown as a function of the measured H^0 scattering angles ($\theta_p = k_{x,H^0}/k_0$, unit millirad). In the left column the theoretical predictions are presented (dashed line: only s^2 contributions, solid line: including non-s^2 contributions) as a function of the inverse impact parameter, which for pure nuclear scattering is proportional to the transverse momentum. The abcissa of both figures can only be qualitatively compared, since in the experimental data above 1.3 mrad the H^0 deflection is due to Rutherford scattering of both nuclei, (thus this regime corresponds to a small impact parameter ≈ 0.1 of the K-shell radius) and below 1 mrad the H^0 is scattered on the electrons only (thus the nuclear-impact parameter should be large (> 1 a.u.)). The striking difference in the calculations for pure s^2 and non-s^2 contributions proves that the puzzling peak first observed by Giese et al.

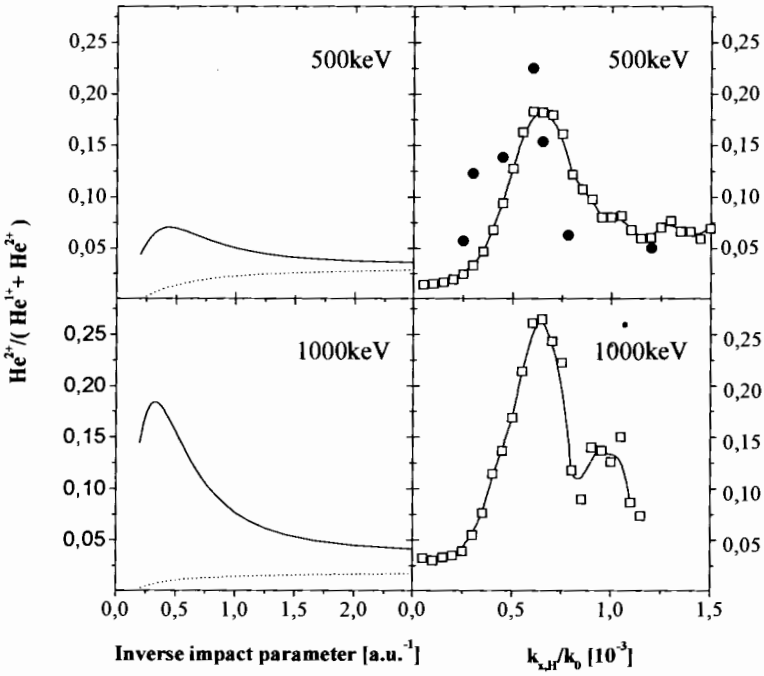

Fig. 20.11. Ratio of H^0 scattering angle ($\theta_p = k_{x,H}/k_0$) TI differential cross sections (this work, *open squares* and Giese and Horsdal, *solid circles*) to the sum of pure capture plus TI cross sections for different projectile energies. (*right column*: experiment, *left column*: theory (see text))

[45] can be related to capture and subsequent shake-off of paired non-s^2 electrons. The theory even gives nice tentative agreement in the absolute height. This indicates that the TuTI process indeed probes the non-s^2 contributions of the ground-state He momentum wave function. It is, however, not possible to reveal the details of the correlated non-s^2 wave function from the measured fully differential cross sections in comparison with theory. We find that the present calculations [40,41] can only partially describe the observed momentum pattern.

Based on a proton straight line trajectory the calculations predict four characteristic features:

1. Only $m = +1$ contributions can be captured into the fast-moving proton. Thus, electron 2 is very asymmetrically emitted (only opposite to the deflected proton towards negative k_x),
2. Momenta of recoil and electron 2 are coplanar in the H^0 scattering plane,
3. At large impact parameters for the impact energies investigated here the non-s^2 contributions to the cKTI process dominate, and
4. For both s^2 and non-s^2 components the emitted electron 2 momentum peaks near zero momentum in the laboratory frame.

Predictions 1., 2., and 3. are in agreement with the data:

- The measured final-state momentum distributions in the nuclear H^0 scattering plane (the nuclear angular momentum vector) are strongly asymmetric below 0.6 mrad, i.e., they show an orientation with respect to the deflected H^0.
- Electron 2 and recoil are coplanar in the H^0 scattering plane.
- The TuTI contribution yields more than 85% of the total TI cross section.

But

- the data are in clear contradiction with the theory, which predicts electrons with low shake-off energy (prediction 4.).

Experimentally we find that TuTI hardly yields electron momenta peaking near zero momentum. As seen in Figs. 20.9 and 20.10, the energy of electron 2 even increases with increasing impact energy and with increasing H^0 angle (below 0.6 mrad). The present theory can not explain why the shake-off electron 2 kinetic energy is of such a large magnitude and, in many cases, exceeding 200 eV.

We note that the non-s^2 angular momentum is not transferred from the proton to any electron, but is provided by the initial He ground state. This conclusion is supported by experimental and theoretical investigations of the pure electron capture process of fast protons on He [43,56]. These authors show that the internal electronic excitation, i.e., the excitation of electron 2 into the p-state of He and the capture of electron 1 into any excited H^0 state is negligibly small for the fast collision systems investigated here. Therefore, the required angular momentum transfer can only be provided from initial-state properties of the captured electron. If the electron is initially in an entangled p^2 or d^2 state the electron 1 can indeed provide the required angular momentum. Since the two electrons have to couple to an $^1S_0$ state, the angular momentum of electron 2 must be antiparallel to that of electron 1 at all times. In classical terms this p or d (or higher ℓ) electron angular momentum $\boldsymbol{\ell}_{e1}$ is pointing perpendicular to the initial plane of motion of the first electron and the motion of the second electron (and α-nucleus) is then confined to the same plane. Since this p or d electron is merged into the H^0 during the capture process, the H^0 must absorb $\boldsymbol{l}_{e1}$ and its deflection (scattering plane) must be perpendicular to $\boldsymbol{l}_{e1}$. Thus, classically, TuTI can only occur if the H^0 scattering plane and the He initial plane of motion are parallel, as observed in our experiments. A TuTI process proceeding via p^2 electrons (with negligibly small momentum and angular momentum exchange between proton and He) could thus indeed explain the observation of a 4-body (p+e1+e2+α-nucleus) coplanar fragmentation.

To further understand the physics behind this TuTI process, we semiempirically reduce the complex pattern to obtain a simpler scaling behavior. To do this, we calculate from the final-state H^0 momentum the initial-state electron 1 momentum. The vectors (black line) in Figs. 20.9 and 20.10 indicate

the mean locations of the initial-state momentum vector (given by 20.2) of the captured electron 1, the vectors (white lines) indicate the mean location of the emitted electron 2 (right column) and the mean location of the emitted α-nucleus in the laboratory frame (left column), respectively.

It should be noted that the vector sum in the laboratory frame of the momenta of all three particles is not zero, since the proton also changes its k_z momentum component ($k_{z,\mathrm{p}} = -m_\mathrm{e}v_\mathrm{p}/2$). The initial-state momentum relation between the three He particles derived from our data is presented in Fig. 20.12, where for nearly all investigated impact energies E_p at three H^0 scattering-angle regimes the measured momentum relation in the CM system is shown (for the smaller H^0 range the energies 150, 200, and 300 keV are not included, since the H^0 transverse momentum resolution was comparable with the measured deflection). It is striking to see that for the TuTI process one always yields more or less the same discrete momentum pattern between the two electrons and the recoil ion, whereas the mean momentum of electron 2 with respect to the projectile momentum in the final state varies strongly with projectile energy and H^0 deflection angle.

In Fig. 20.12, the initial-state vector k_{e1} is plotted. Its length for the different $E_\mathrm{p}(m_\mathrm{e}v_\mathrm{p})$ is set equal to one. For all systems investigated the relative angle $\theta_{\mathrm{e1-e2}}$ between electron 1 and 2 appears constant with $\theta_{12} = 140° \pm 25°$ and the angle between electron 2 and the recoil ion is $\theta_{\mathrm{e2}} - \theta_{recoil} = 70° \pm 25°$. Also the ratios of the momentum vector magnitudes are constant within the experimental uncertainty of about 30%.

20.5 Conclusions

We conclude that the puzzling structures observed by Mergel et al. [18] and Giese et al. [45] can be qualitatively explained by the TuTI process proceeding via selected shake-off processes from non-s^2 components in the asymptotic part of the He ground-state wave function. Several experimental observations can be qualitatively explained by the theory:

1. the puzzling peak in the angle-dependent ratio of TI to sum of TI+ capture
2. the observed asymmetry in electron 2 emission, and
3. the coplanar emission pattern of recoil electron 2 and scattered H^0.

However, the large electron 2 momenta and the striking general scaling of the momentum distributions shown in Fig. 20.12 are in clear contradiction to theory. It is interesting to note that in classical mechanics such a scaling was predicted for the He ground state by [57]. When the two He electrons move on two opposite (180°) elliptic orbits with the nucleus at rest, they can never fulfill simultaneously momentum and angular momentum conservation. They need a nucleus for compensation of momentum (strong phonon coupling), which is then more easily fulfilled, if the axes of the electron ellipses are not

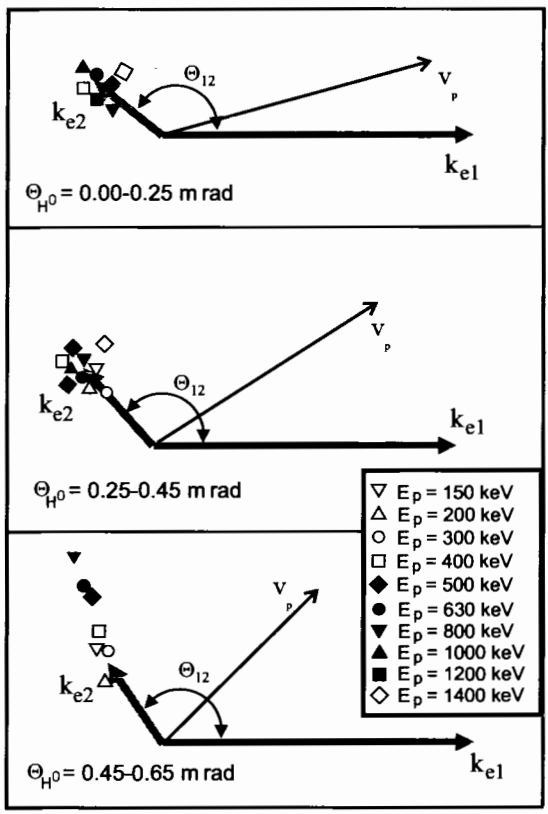

Fig. 20.12. The measured *initial state* momentum relation ($\Longrightarrow$ correlated asymptotic momentum wave function) of the two electrons is shown for three H^0 scattering-angle regimes for all the indicated proton energies. The momentum vector k_{e1} of the captured electron 1 is always set to (1,0) for all proton impact energies E_p. Its determination is described in the text (see (20.2))

intersecting by 180° but, as suggested by Sommerfeld (1923) [57], by a smaller angle between 90° and 150°.

Experimentally we find: electron 2 is always emitted into polar angles of about 140° ± 25° with respect to electron 1 with a well-defined relative velocity, i.e., the entangled three-particle momentum wave function shows a semi-quantized structure. Furthermore, we have shown that the non-s^2 contributions in the He ground-state wave function are not purely mathematical constructs in the virtually exited space, but have measurable consequences. These off-diagonal non-s^2 components seem to hide interesting properties with respect to the secret world of correlation. These states have classically seen a huge amount of kinetic energy, thus they are called highly virtually

excited continuum states. These very fast electrons at large distance from the He nucleus are those with the strongest dynamical e–e correlations.

Classically seen, here the negative Coulombic energy is more than a factor of 10 smaller than the positive kinetic energy of the fast electrons in a non-s^2 state. Since the kinematical capture observed here can only occur when the electron 1 velocity (absolute value) matches the projectile velocity, this TuTI process at a given v_p sets a narrow window on the captured electron velocity and therefore provides a powerful method for viewing selectively very high momentum components ($< 10^{-6}$ fractions of the global wave function) in the He ground state, which are not observable in even the most precise binding energy measurements. Both electrons occupy the non-s^2 state of motion together simultaneously with the nucleus, since the He ground state is a $^1S_0$ state.

Generally one would call such a two-electron system a pairing state (e.g., like a Cooper pair in a solid), however, this is misleading and overlooks the most important reason for that entanglement. It is the coupling of both electron momenta and angular momenta to the nuclear motion (the nucleus is never at rest). It is well known for superconductivity that phonon coupling to the solid (isotope effects) is very important. We see here for the He system that beside entanglement in momentum ($\Longrightarrow$ phonon coupling) the angular momentum entanglement is even more important. Therefore, also for superconductivity and the quantized Hall effect (in particularly, the fractional Hall effect) angular momentum entanglement might be crucial for the existence of such dynamically entangled systems.

Acknowledgements

We acknowledge the numerous fruitful disputes and discussions with our colleagues and friends: U. Ancarani, D. Belkić, J. Berakdar, S. Berry, J. Briggs, S. Brodzki, H. Cederquist, R. Dreizler, J. Feagin, B. Fricke, S. Fritsche, C. Greene, W. Greiner, J. McGuire, S. Hagmann, M. Horbatsch, O. Jagutzki, E. Horsdal, P. Hoyer, D. Ionescu, D. Madison, J. Macek, S. Manson, R. Moshammer, C.D. Lin, R. Olson, Yu. Popov, J. Reading, R. Rivarola, J.M. Rost, H. Schmidt, V. Schmidt, R. Schuch, J. Ullrich, and many other colleagues.

V.M. acknowledges the support by the Studienstiftung des Deutschen Volkes, and E.W. by the Humboldt-Stiftung. This work was supported by the DFG, the BMBF, GSI-Darmstadt, Graduiertenprogramm des Landes Hessen, DAAD and Roentdek GmbH.

References

1. T. Kinoshita: Phys. Rev. **115**, 366 (1959)
2. G. W. F. Drake: in *Long Range Casimir Forces: Theory and Recent Experiments on Atomic Systems*. Eds. F.S. Levin, D.A. Micha (Plenum, New York 1994) p. 107
3. S. D. Bergeson et al.: Phys. Rev. Lett. **80**, 3475 (1998)
4. A. T. Stelbovics: Invited paper, Proceedings of ICPEAC 1991, Eds. W. R. MacGillivray, I. E. McCarthy, M. C. Standage (IOP, Bristol) p. 21, SSBN 0-7503-0167-8
5. W. C. Fon, K. A. Berrington, P. G. Burke, A. E. Kingston: J. Phys. B **14**, 1041 (1981)
6. T. T. Scholz, H. R. J. Walters, P. G. Burke, M. P. Scott: J. Phys. B **24**, 2097 (1991)
7. G. Tanner, K. Richter, J. M. Rost: Rev. Mod. Phys. **72**, 497 (2000)
8. J. P. D. Cook, I. E. McCarthy, A. T. Stelbovics, E. Weigold: J. Phys. B **21**, 2415 (1984)
9. Y. F. Smirnov, A. V. Pavlitchenkov, V. G. Levin, V. G. Neudatschin: J. Phys. B **11**, 1587 (1978)
10. V. G. Levin, V. G. Neudatchin, A. V. Pavlitchankov, Y. F. Smirnov: J. Phys. B **17**, 1525 (1984)
11. J. S. Briggs, V. Schmidt: J. Phys. B **33**, R1 (2000)
12. A. Dorn, R. Moshammer, C. D. Schröter, T. J. M. Zouros, W. Schmitt, H. Kollmus, R. Mann, J. Ullrich: Phys. Rev. Lett. **82**, 2496 (1999)
13. A. Dorn, A. Kheifets, C.D. Schröter, B. Najjari, C. Höhr, R. Moshammer, J. Ullrich: Phys. Rev. Lett. **86**, 3755 (2001)
14. I. Taouil, A. Lahmam-Bennani, A. Duguet, L. Avaldi: Phys. Rev. Lett. **81**, 4600 (1998)
15. J. Macek: Z. Phys. D **3**, 31 (1986)
16. V.M. Efimov: Comments Nucl. Part. Phys. **19**, 271 (1990)
17. A. Lahmam-Bennani, C. C. Jia, A. Duguet, I. Avaldi: J. Phys. B **35** L215 (2002)
18. V. Mergel, R. Dörner, K. Khayyat, M. Achler, T. Weber, O. Jagutzki, H.J. Lüdde, C.L. Cocke, H. Schmidt-Böcking: Phys. Rev. Lett. **86**, 2257 (2001)
19. R. Dörner, V. Mergel, O. Jagutzki, L. Spielberger, J. Ullrich, R. Moshammer, H. Schmidt-Böcking: Phys. Rep. **330**, 96 (2000)
20. J. Ullrich, R. Moshammer, R. Dörner, O. Jagutzki, V. Mergel, H. Schmidt-Böcking and L. Spielberger: J. Phys. B: At. Mol. Opt. Phys. **30**, 2917 (1997)
21. V. Mergel, R. Dörner, M. Achler, K. Khayyat, S. Lencinas, J. Euler, O. Jagutzki, S. Nüttgens, M. Unverzagt, L. Spielberger, W. Wu, R. Ali, J. Ullrich, H. Cederquist, A. Salin, R.E. Olson, D. Belkić, C.L. Cocke, H. Schmidt-Böcking: Phys. Rev. Lett. **79**, 387 (1997)
22. J. Palinkas, R. Schuch, H. Cederquist, O. Gustafsson: Phys. Rev. Lett. **63**, 2464 (1989)
23. J. S. Briggs, K. Taulbjerg: J. Phys. B **12**, 2565 (1979)
24. T. Ishihara, J.H. McGuire: Phys. Rev. A **38**, 3310 (1988)
25. J. H. McGuire, J.C. Straton, W. J. Axmann, T. Ishihara, E. Horsdal: Phys. Rev. Lett. **62**, 2933 (1989)
26. J. H. McGuire, N. Berrah, R. J. Bartlett et al.: J. Phys. B **28**, 913 (1995)

27. R. Shakeshaft, L. Spruch: Rev. Mod. Phys. **51**, 369 (1979)
28. L. H. Thomas: Proc. Roy. Soc. A **114**, 561 (1927)
29. E. Horsdal-Pedersen, C. L. Cocke, M. Stöckli: Phys. Rev. Lett. **50**, 1910 (1983)
30. H. Vogt, R. Schuch, E. Justiniano, M. Schulz, W. Schwab: Phys. Rev. Lett. **57**, 2256 (1986)
31. J. C. Levin, D. W. Lindle, N. Keller, R. D. Miller, Y. Azuma, N. Berrah Mansour, H. G. Berry, I.A. Sellin: Phys. Rev. Lett. **67**, 968 (1991)
32. L. Spielberger, O. Jagutzki, R. Dörner, J. Ullrich, U. Meyer, V. Mergel, M. Unverzagt, M. Damrau, T. Vogt, I. Ali, K. Khayyat, D. Bahr, H. G. Schmidt, R. Frahm, H. Schmidt-Böcking: Phys. Rev. Lett. **74**, 4615 (1995)
33. L. Spielberger, O. Jagutzki, B. Krässig, U. Meyer, K. Khayyat, V. Mergel, T. Tschentscher, T. Buslaps, H. Bräuning, R. Dörner, T. Vogt, M. Achler, J. Ullrich, D.S. Gemmell, H. Schmidt-Böcking: Phys. Rev. Lett. **76**, 4685 (1996)
34. L. Spielberger, H. Bräuning, A. Muthig, J.Z. Tang, J. Wang, Y. Qui, R. Dörner, O. Jagutzki, T. Tschentscher, V. Honkimäki, V. Mergel, M. Achler, T. Weber, K. Khayyat, J. Burgdörfer, J. McGuire, H. Schmidt-Böcking: Phys. Rev. A **59**, 371 (1999)
35. J. C. Levin, G. B. Armen, I. A. Sellin: Phys. Rev. Lett. **76**, 1220 (1996)
36. F. W. Byron, C.J. Joachain: Phys. Rev. A **164**, 1 (1967)
37. L. R. Andersson, J. Burgdörfer: Phys. Rev. Lett. **71**, 50 (1993)
38. E. G. Drukarev, N.B. Avdonina, R.H. Pratt: J. Phys. B **34**, 1 (2001)
39. V. Mergel: PhD Thesis, Universität Frankfurt, Shaker Verlag, ISBN 3-8265-2067-X (1996)
40. A. S. Kheifets: private communication, 2003 (to be published)
41. T. Y. Shi, C. D. Lin: Phys. Rev. Lett. **89**, 163202 (2002)
42. R. Gayet, A. Salin: J. Phys. B **20**, L571 (1987)
43. R. Gayet, A. Salin: Nucl. Instrum. Methods B **56**, 82 (1991)
44. E. Horsdal, B. Jensen, K.O. Nielsen: Phys. Rev. Lett. **57**, 1414 (1986)
45. J. P. Giese, E. Horsdal: Phys. Rev. Lett. **60**, 2018 (1988)
46. R. E. Olson, J. Ullrich, R. Dörner, H. Schmidt-Böcking: Phys. Rev. A **40**, 2843 (1989)
47. R. Gayet: J. de Phys., **C1-53**, 70 (1989)
48. R. Gayet, A. Salin: in *High-Energy Ion-Atom-Collisions* Proc. of the 4th Workschop, Debrecen Sept. 1990, eds. D. Bereny and G. Hock (Lecture Notes in Physics; Vol. 376) (Springer, Berlin, Heidelberg, New York 1991) (1990)
49. M. B. Shah, H.B. Gilbody: J. Phys. B **18**, 899 (1985)
50. E. Horsdal, B. Jensen, K.O. Nielsen: Phys. Rev. Lett. **57**, 675 (1986)
51. H. T. Schmidt et al.: Phys. Rev. Lett. **89**, 163201 (2002)
52. J. Ullrich, R. Moshammer, H. Berg, R. Mann, H. Tawara, R. Dörner, J. Euler, H. Schmidt-Böcking, S. Hagmann, C.L. Cocke, M. Unverzagt, S. Lencinas, V. Mergel: Phys. Rev. Lett. **71**, 1697 (1993)
53. F. G. Kristensen and E. Horsdal-Pedersen: J. Phys. B **23**, 4129 (1990)
54. W.R. DeHaven, C. Dilley, A. Landers, E.Y. Kamber: Phys. Rev. A **57**, 292 (1998)
55. P. Sigmund, K.B. Winterbon: Nucl. Instrum. Methods **119**, 541 (1974)
56. V. Mergel: Diplomarbeit Universität Frankfurt (1994)
57. A. Sommerfeld: J. Opt. Soc. Am. **7**, 509 (1923)